Upper Critical Fields of the Superconducting Layered Compounds $Nb_{1-x}Ta_xSe_2$

B. J. Dalrymple and D. E. Prober

Section of Applied Physics, Becton Center, Yale University, New Haven, Connecticut

The upper critical fields $H_{c2}(T)$ of the superconducting layered compounds $Nb_{1-x}Ta_xSe_2$ ($0 \leq x \leq 0.20$) have been measured with the magnetic field oriented either perpendicular or parallel to the layer plane. Just below T_c, positive (upward) curvature is seen in $H_{c2}(T)$ for both field directions and for all compositions. The amount of positive curvature is not a function of crystal quality. At low temperatures, $H_{c2}(T)$ displays enhanced linearity as compared to the prediction of the isotropic theory, and shows no evidence of Pauli paramagnetic limiting for either field orientation. The critical field slopes dH_{c2}/dT near T_c change only slightly with composition. $H_{c2}(T)$ has been calculated for two Fermi surface models for $NbSe_2$ using the band structure calculated by Wexler and Woolley. These $H_{c2}(T)$ calculations indicate that Fermi surface anisotropy can explain the positive curvature and enhanced linearity seen in the experimental data. The calculations also show that the $H_{c2}(T)$ data are better explained with a Fermi surface that consists of open, undulating cylinders with an additional smaller closed piece, than with a Fermi surface model that consists only of the open, undulating cylinders of the original Wexler and Woolley model.

1. INTRODUCTION

This paper reports measurements of the upper critical fields $H_{c2}(T)$ of the superconducting transition-metal dichalcogenide compounds $Nb_{1-x}Ta_xSe_2$ ($0.0 \leq x \leq 0.20$).* The physical properties of these compounds are generally of interest because the layered crystal structure, similar to that of graphite, can produce very anisotropic electronic properties. Many previous studies of the upper critical fields of the superconducting layered compounds have been concerned with intercalated materials, which have a layer of organic molecules inserted between the metallic layers. (The $NbSe_2$ crystals we have studied were not intercalated.) For the intercalated

---

*A more detailed account of this work can be found in Ref. 1.

compounds, it is possible to observe a crossover to quasi-two-dimensional critical field behavior when the magnetic field is oriented parallel to the layer plane.[2,3] Dimensional crossover effects are not seen in the unintercalated compounds, due to their less extreme anisotropy. Still, these materials are of interest as models for studying how real-metal effects, such as Fermi surface anisotropy, can influence the superconducting properties. The upper critical fields display a number of novel effects, some of which have not been satisfactorily explained by previous studies. These novel effects for H_{c2} include positive curvature near T_c and enhanced linearity at low temperatures, in addition to the expected orientational anisotropy. The study and interpretation of these properties provide the subject of the present work.

The upper critical fields of $NbSe_2$ have been investigated by a number of researchers.[4-10] The temperature dependence of $H_{c2}(T)$ with the magnetic field oriented perpendicular ($\perp$) and parallel ($\parallel$) to the layer plane was first reported by Foner and McNiff.[4] They observed an orientational anisotropy of ~3, and also that $H_{c2}(T)$ displays extended linearity at low temperatures when compared to the shape of $H_{c2}(T)$ predicted by the isotropic theory. Subsequent investigations have confirmed these observations. Most workers have reported positive (upward) curvature just below T_c for the parallel critical field $H_{c2\parallel}(T)$,[5,6,10] in contrast to the conventional linear dependence, $H_{c2} \propto (T_c - T)$. The experimental findings on curvature of the perpendicular critical field $H_{c2\perp}(T)$ were, prior to the present work, less clear. The extremely detailed measurements of $H_{c2}(T)$ we have made near T_c indicate that positive curvature exists for both field orientations, although the magnitude of the effect is larger for $H_{c2\parallel}(T)$.

The main theoretical framework used to interpret almost all of the previous experiments on $NbSe_2$ is the anisotropic Ginzburg–Landau (GL) theory.[11,12] (See also the discussion in Ref. 2.) In the anisotropic GL model, the effective pair mass is assumed to be anisotropic, leading to anisotropic coherence lengths and thus anisotropic critical fields. In general, the experimental results are in good *qualitative* agreement with the theoretical predictions of this model. However, many of the specific features of the critical fields cannot be explained within the anisotropic GL theory. Examples are the extended linearity of H_{c2} well below T_c and the positive curvature just below T_c. It is of interest to see whether these features indicate novel superconductivity mechanisms or interactions (such as the interaction of the superconducting order parameter with the charge density wave), or whether the explanation of these features is instead provided by careful calculations using just the conventional microscopic theory of superconductivity, but generalized to include anisotropy. We conclude that the latter, more prosaic, explanation applies for the compounds and properties we have studied.

Positive curvature and enhanced linearity are ubiquitous features of H_{c2} for many newly discovered crystalline superconductors, including the layered dichalcogenides, intercalated graphite, and A-15 superconductors.[13] It was widely held that there was no satisfactory explanation (see, however, our comments below on the theoretical work by Takanaka). With our results, it is clear that, at least for NbSe$_2$ and its Ta alloys, these puzzling features of the $H_{c2}(T)$ curves are explainable within conventional microscopic theory, once the microscopic band structure is carefully considered.

Recently a calculation of H_{c2} for NbSe$_2$, based on microscopic theory, was presented by Takanaka.[14] He found that for a cylindrical Fermi surface, $H_{c2\parallel}(T)$ could show upward curvature and extended linearity. However, $H_{c2\perp}(T)$ did not display these features. This is consistent with our findings for such a Fermi surface.[1] The parameters that Takanaka needed to fit the temperature dependence of $H_{c2\parallel}(T)$ were not fully acceptable. These discrepancies, identified by Takanaka, do not appear to be that problematic, as the actual Fermi surface is more complicated than the straight cylinder he considered; this is discussed fully in Section 5.

The experimental goal of this research was to study $H_{c2}(T)$ of a series of anisotropic compounds in which the composition could be varied via substitutional alloying. NbSe$_2$ is a convenient starting point for such an investigation, since many of its properties, in addition to the upper critical fields, have previously been investigated. Also, it is possible to grow high-quality NbSe$_2$ crystals. Changing the composition by substitutional alloying allows the electron mean free path (as well as other material properties) to be varied in a systematic manner. Since Nb and Ta have similar atomic radii and similar electronic and chemical properties, substitutional alloying should work well in the Nb$_{1-x}$Ta$_x$Se$_2$ system. Indeed, we find that it is possible to produce high-quality crystals of this alloy system.

The upper critical fields of the alloy series Nb$_{1-x}$Ta$_x$Se$_2$ have previously been studied by Ikebe *et al.*[10] and our data generally agree with theirs. However, we present much more detailed results, for a larger number of compositions. This allows a more systematic and quantitative study of the dependence of the critical fields upon composition, and resolution of certain issues not resolved by Ikebe, such as the effect of the charge density wave on H_{c2}. Ikebe *et al.* based their analysis on the anisotropic GL theory. We have calculated $H_{c2}(T)$ instead using *microscopic* theory, incorporating realistic Fermi surface models. This allows a quantitative comparison of the predictions of these Fermi surface models with the experimental data. Such testing of Fermi surface models is not possible with an analysis based on the anisotropic Ginzburg–Landau theory.

In the course of this work we have found that the available theory and formulations for calculating H_{c2} in anisotropic systems are not fully developed. The question of how to treat the simultaneous occurrence of

Fermi surface anisotropy, electron scattering, strong coupling effects, energy gap anisotropy, and Pauli paramagnetism with spin–orbit scattering is not presently resolved. We have therefore needed to improvise and generalize from the isotropic theory for type II superconductors, where some of these issues have, at least individually, been explored. Thus, while not all aspects of our results can be analyzed in full, we believe that the extensive data set we present will prove useful for testing future theoretical advances relating to anisotropic superconductors.

This paper begins with a brief description of the techniques used to grow single-crystal specimens and to measure the superconducting-to-normal phase transition. The main body of the paper concentrates on the presentation and analysis of the critical field results.

2. CRYSTAL STRUCTURE AND GROWTH

The crystal structure of the transition metal dichalcogenides consists of three-atom-thick, covalently bonded layers with weak van der Waals-type interlayer bounding. Each layer consists of three hexagonal close-packed planes of atoms; a plane of metal atoms is sandwiched between two planes of chalcogen atoms (S, Se, or Te). The individual planes and layers can be stacked in a variety of ways, resulting in different crystal structures, or polytypes.[15] Except where noted, all the results in this paper are for the 2H phase, which has a unit cell with a two-layer repeat distance and trigonal prismatic coordination of the metal atoms by the surrounding chalcogen atoms. The flat hexagonal-platelet crystal morphology reflects the microscopically layered crystal structure.

The standard method of producing single crystals of the transition metal dichalcogenides is the vapor-transport technique, which we have also used. In almost all previous studies iodine was used as the transport agent. Most of the crystals grown for this study were instead produced using selenium as the transport agent.[16] Selenium transport can produce better quality crystals, and ensures that there is no iodine contamination. Preparation procedures are also simpler than with iodine transport. We have developed systematic and reproducible procedures for accomplishing Se vapor transport. A detailed description of these crystal growth procedures will be reported elsewhere.[17]

For crystal growth by Se transport, temperatures in the growth zone of the crystal-growth tube were between 700 and 750°C, with a temperature difference of (typically) 20°C between the hot and cold zones. As the Ta content is increased, it is necessary to use slightly lower crystal-growth temperatures to avoid forming the 4H phase, which is stable at higher temperatures. Excess Se is not incorporated into the crystals at the growth

temperatures used. (At lower temperatures, triselenides will form if excess Se is present.) The crystallographic phase obtained for a particular set of crystal-growth conditions was verified by x-ray diffraction analysis.

3. EXPERIMENTAL TECHNIQUES

We have found that the best quality Nb$_{1-x}$Ta$_x$Se$_2$ crystals are fairly small. Using the superconducting transition width and the smoothness of the transition curve as measures of crystal quality, it appears that the best crystals are thin hexagonal platelets with diameters between 0.1 and 1.0 mm and thicknesses on the order of 15 μm.

A very sensitive ac susceptibility apparatus was developed for measuring the superconducting-to-normal phase transition of such small samples. This apparatus is shown schematically in Fig. 1. The sample is placed inside a small copper pickup coil L, which is part of a high-Q ($Q > 30$) LC parallel resonant circuit. The rf magnetic field is perpendicular to the sample face for either orientation of the dc magnetic field (Fig. 1a). The LC circuit is driven by a rf current source at a frequency near resonance ($f_r = 2$–3 MHz). The rf current source consists of a rf voltage generator, Hewlett-Packard 606A, in series with a 1-pF capacitor. The voltage across the LC circuit is proportional to its impedance. This voltage is fed into a phase-sensitive detector, which, because of the phase shift across the 1-pF capacitor, produces a dc output voltage proportional to the *imaginary* component of the LC circuit impedance Z_{LC}. This component of Z_{LC} is zero at f_r and varies linearly and rapidly near resonance, as shown in Fig. 1b.

If the magnetic properties of the sample change, e.g., as the temperature is raised through the superconducting transition, the resonant frequency will shift. The sample's magnetic susceptibility in the superconducting state is diamagnetic, due to shielding currents that flow to shield the applied rf magnetic field. These shielding currents can be caused by an intrinsic barrier to flux entry[1,18] or by flux pinning. In the normal state [$T > T_{c2}(H)$], the magnetic susceptibility is nearly zero for small samples, in the absence of surface superconductivity effects (discussed below). The sharp change in the ac susceptibility at $H_{c2}(T)$ [or $T_{c2}(H)$] changes the resonant frequency and thus translates the whole curve in Fig. 1b horizontally. The dc output voltage thus also shifts, since the circuit is biased at a fixed frequency.

This apparatus is sufficiently sensitive to detect the superconducting transition in a sample that is a thin, hexagonal platelet 50 μm in diameter and approximately 10 μm thick (mass 0.13 μg) with a signal-to-noise ratio of 20. The main source of noise is the rf amplifier. The ac field strengths used are between 0.01 and 0.1 G; these ac field magnitudes do not depress the observed transition. The excellent sensitivity of this apparatus allows
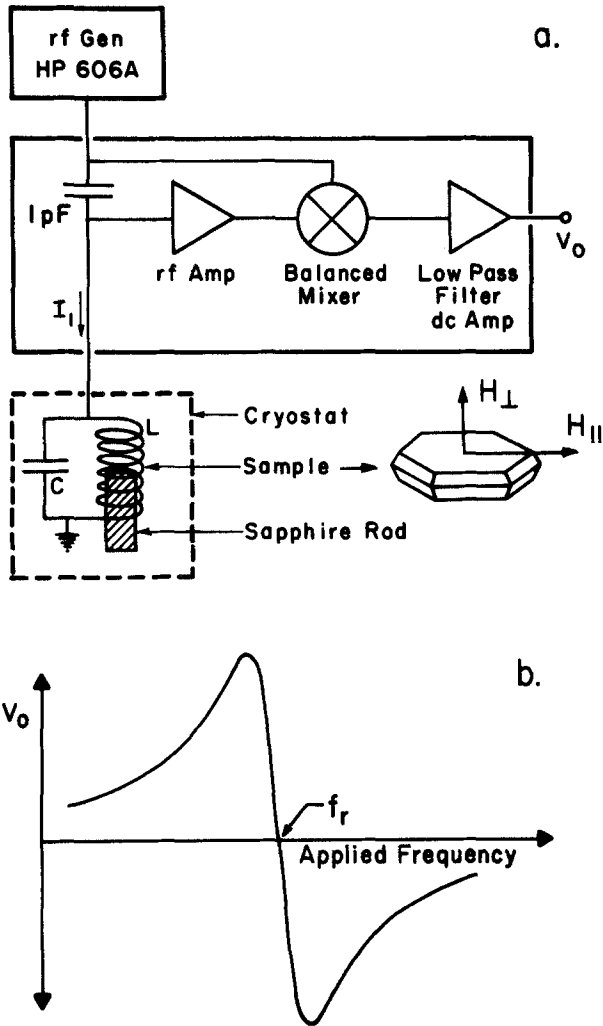
Fig. 1. (a) Block diagram of the phase-sensitive detector used to measure shifts in the resonant frequency of the parallel LC circuit. The sample is mounted in the coil L on a sapphire rod in a variable-temperature cryostat. A hexagonal-platelet sample is shown, indicating the orientation of the dc magnetic field perpendicular ($\perp$) and parallel ($\parallel$) to the face of the sample. (b) The output voltage V_0 as a function of rf generator frequency. The circuit is biased at a fixed frequency near resonance, on the linear portion of the curve. If the magnetic properties of the sample change, the resulting shift in the resonant frequency will be translated into a shift in V_0.

samples to be selected solely on the basis of crystal quality, without any constraint on sample size. A detailed description of the electronics and the variable-temperature cryostat is given elsewhere.[1,19]

Susceptibility data were taken by sweeping the temperature in a constant dc field. Zero-field temperatures were measured using a calibrated germanium resistance thermometer. A capacitance thermometer was used in large dc fields. Magnetic fields to 80 kG were provided by a Nb–Ti superconducting magnet, operated in the persistent mode. Experiments have also been carried out to 150 kG, at the Francis Bitter National Magnet Laboratory of the Massachusetts Institute of Technology.

In using ac susceptibility transitions for determing H_{c2}, one must establish that the observed transitions occur at $H_{c2}(T)$ for the class of materials being studied. Two pieces of evidence confirm this relationship between susceptibility transitions and the location of H_{c2} for our samples. The most significant evidence is that the ac susceptibility transitions we observe for $NbSe_2$ in a perpendicular field agree with specific heat measurements of $H_{c2\perp}$ by Schwall et al.[7] and Garoche et al.[8] (See Table I, below.) Such specific heat measurements are true bulk measurements, and reliably establish $H_{c2}(T)$ [or $T_{c2}(H)$]. The specific heat studies were done with larger crystals than were studied here. The second piece of evidence is that when the dc field is oriented parallel to the surface of the thin platelet samples, a small tail is often observed in the ac susceptibility data at temperatures above the main transition. The temperature at which this tail terminates scales as predicted by the theory of surface superconductivity ($H_{c3} \sim 1.7 H_{c2}$). No specific heat data are available for parallel fields. Our observation of a small surface superconductivity effect for the parallel field orientation further reinforces our identification that the main susceptibility transition occurs at $H_{c2}(T)$.

4. EXPERIMENTAL RESULTS

This section presents the main experimental results. We begin with a discussion of the transition temperature and transition width as a function of composition, followed by a discussion of the critical field data. Over the composition range studied here, the critical fields of $Nb_{1-x}Ta_xSe_2$ do not change greatly as a function of alloy composition. Therefore, we first present those critical field properties that are largely independent of composition, and then discuss how the various parameters change as a function of composition.

4.1. Zero-Field results: T_c and Transition Width

Figure 2 shows the transition temperature of $Nb_{1-x}Ta_xSe_2$ as a function of x (see also Tables I and II). The T_c is defined by the midpoint of the
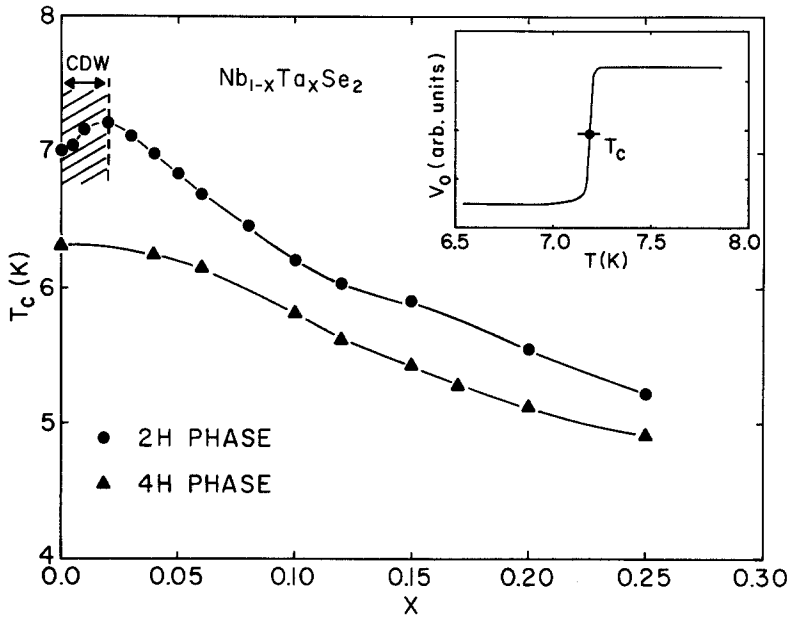
Fig. 2. The transition temperature as a function of composition for the 2H and 4H phases. The inset shows a zero-field transition curve for a sample of $Nb_{0.99}Ta_{0.01}Se_2$ and the definition of T_c as the midpoint of the transition curve. For the 2H phase, the zero-field transition widths are typically 30–50 mK, smaller than the dots used in this figure.

TABLE I

Comparison of Data for 2H $NbSe_2$

Author	T_c, K	RRR	$dH_{c2\perp}/dT$,[a] kG/K	$dH_{c2\parallel}/dT$,[a] kG/K
This work	7.01	41[b]	6.60	21.5
Foner and McNiff[4]	—	—	7.9	25.7
Leupold et al.[6]	7.14	—	8.73	30.0
	7.27	—	7.82	23.3
Prober et al.[2]	7.19	—	8.0	23
Schwall et al.[7]	7.1	—	6.45	—
Toyota et al.[5]	7.18	33	6.96	16.43
	7.29	32	7.27	18.24
	7.34	30	6.54	16.35
	7.39	35	7.04	16.91
Garoche et al.[8]	7.11	46	6.9	—
Ikebe et al.[10]	7.29	32	7.7	27.5

[a] The slopes tabulated here are for the main linear section of the $H_{c2}(T)$ curves.
[b] Measured on a large crystal.

TABLE II
Properties of $Nb_{1-x}Ta_xSe_2$

Composition, at% Ta	T_c, K		RRR^a (2H)	$H_{c2\parallel}/H_{c2\perp}$ (at $t=1/2$)
	2H	4H		
0.0	7.01	6.31	41	3.1
0.5	7.05	—	—	3.17
1.0	7.17	—	—	3.18
2.0	7.22	—	—	3.23
3.0	7.12	—	—	—
4.0	6.99	6.24	—	3.27
5.0	6.85	—	16, 20	3.29
6.0	6.69	6.14	—	—
8.0	6.46	—	—	—
10.0	6.21	5.81	7.6	3.42
12.0	6.03	5.61	—	—
15.0	5.90	5.42	—	—
17.0	—	5.28	—	—
20.0	5.55	5.12	4.9^b	3.66
25.0	5.22	4.91	—	—

[a] The basal-plane residual resistance ratio is defined as the room-temperature resistance divided by the resistance just above T_c.
[b] Reference 10.

measured transition curve. The zero-field transition widths (10% to 90%) are typically 30–50 mK and do not depend upon composition. Data are also shown in Fig. 2 for T_c of the 4H phase. The critical fields of the 4H phase were not studied, as high-quality crystals of this material are more difficult to produce, and the relevant normal-state properties (e.g., the Fermi surface) have not been investigated. The 4H phase will not be discussed further.

For the 2H phase there is, overall, a decrease in T_c as the Ta content is increased from $x=0$ to $x=0.20$. However, for small Ta concentrations, T_c initially increases with x. This appears to be caused by suppression of the charge-density wave (CDW) found in pure $NbSe_2$.[15,20] The CDW introduces gaps into the band structure at the Fermi level. These gaps decrease the electronic density of states, thus lowering T_c. It is known that the CDW in $NbSe_2$ is suppressed by pressure[21] and by lattice disorder.[22–24] Extrapolating the T_c versus pressure data[21] linearly back to atmospheric pressure indicates that in the absence of a CDW, T_c of $NbSe_2$ might be about 7.9 K. In our samples the disorder leading to CDW suppression is caused by the random substitution of Ta atoms for Nb atoms.

Further evidence for the sensitivity of the CDW to lattice disorder is supplied by our observation that if crystals with compositions to the left of

the peak in the T_c curve ($x \lesssim 0.02$) are slightly damaged, their transition curves are broadened, and a high-temperature tail appears in the zero-field susceptibility data. Observed tails extend to $\lesssim 7.4$ K. This behavior is not seen for compositions to the right of the peak, where we argue that the CDW is suppressed. [Crystal damage was (unintentionally) produced by gluing the samples rigidly to sapphire sample-mounting rods with GE 7031 varnish, followed by rapid thermal cycling. Mounting the samples with rubber cement ('Grippit') diluted with hexane, and slow thermal cycling minimized the chance of crystal damage. This improved mounting technique was used in all our later work.] We conclude that if the CDW were absent in $NbSe_2$, T_c would be ~7.4–7.5 K at atmospheric pressure. Substitutional alloying of Ta would then decrease T_c in a uniform and simple fashion, matching well onto the behavior seen for $x \gtrsim 0.03$. We note that T_c values up to 7.4 K have been reported for (apparently damaged) $NbSe_2$.

Based on the above considerations, it appears that higher quality $NbSe_2$ crystals should have *lower* transition temperatures,[23] since more perfect crystals have stronger CDWs and the CDW depresses T_c. The range of T_c values reported in the literature for $NbSe_2$ is fairly large, ranging from 6.95 K[25] to approximately 7.4 K[4,5] (ignoring anomalously low values, which appear to be caused by severe crystalline imperfection or incorporation of excess Nb into the crystal structure[26]). The crystals used in our work were grown in an environment with a very slight excess of Se, to ensure correct stoichiometry.[20] The sensitivity of the CDW to crystalline imperfection appears to account, at least in part, for the range of T_c values in the literature. Based on our measurements, we believe that values of T_c in the range 6.96–7.05 K are characteristic of high-quality, undamaged $NbSe_2$ crystals.

4.2. $H_{c2}(T)$ As a Function of Temperature and Field Orientation: Composition-Independent Features

In this section we discuss the shapes of the critical field curves, which change only slightly as a function of composition. Figure 3 shows $H_{c2}(T)$ for a sample of composition $Nb_{0.99}Ta_{0.01}Se_2$ with the field orientated perpendicular ($\perp$) and parallel ($\parallel$) to the layer plane. The $H_{c2}(T)$ curves of Fig. 3 are representative of all the compositions studied. Within an uncertainty of 2% in $H_{c2}(T)$, we find no anisotropy when the field is rotated in the basal plane. The transition temperature $T_{c2}(H)$ is defined as the midpoint of the transition curve (inset, Fig. 3a). However, all the features discussed below are independent of the exact definition of $T_{c2}(H)$; we would draw the same conclusions, for example, if we were to use the onset temperature of the main portion of the superconducting transition. The transition widths
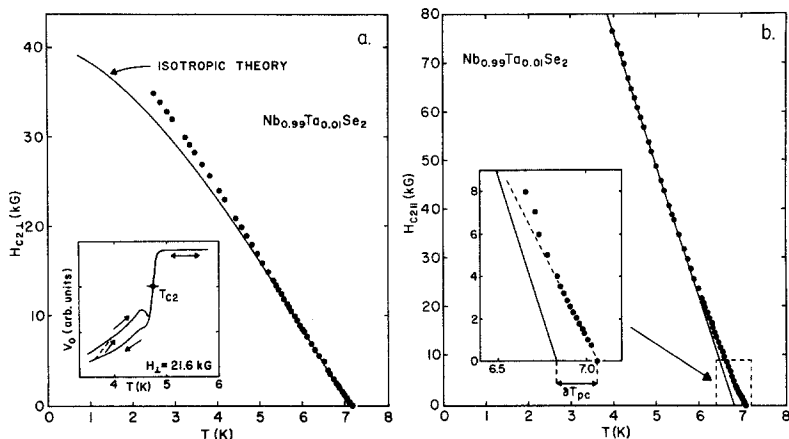
Fig. 3. (a) The perpendicular critical field of $Nb_{0.99}Ta_{0.01}Se_2$. Also shown is the temperature dependence of the isotropic, clean-limit theoretical curve scaled to achieve an approximate best fit. The inset shows a transition curve in a perpendicular dc magnetic field, showing the definition of $T_{c2}(H)$ as the midpoint of the linear portion of the transition. The arrows indicate the direction of the temperature sweep. The hysteresis seen in the mixed state, below the transition, is an intrinsic phenomenon and is discussed in the text. (No hysteresis is seen in the zero-field transition curves—Fig. 2, inset.) (b) The parallel critical field of $Nb_{0.99}Ta_{0.01}Se_2$. Shown is a straight line fit to the main linear portion of the $H_{c2\parallel}(T)$ curve. The amount of positive curvature δT_{pc} can be quantified as the difference between the measured zero-field T_c and the intercept of this solid straight line with the temperature axis, as shown in the inset. The inset shows $H_{c2\parallel}(T)$ near T_c on an expanded scale. The dahed line in the inset indicates the apparent linearity of $H_{c2\parallel}(T)$ very close to T_c.

increase with the applied field, but only to 0.15 K (typical) at the lowest temperature achieved, ∼1.4 K.

The inset in Fig. 3a shows that the ac susceptibility data are hysteretic at temperatures below the main transition, in the mixed state. This behavior is probably caused by an intrinsic barrier to flux entry into a type II superconductor in the mixed state.[18] The surface barrier to flux exit can be smaller in magnitude. An asymmetric barrier could affect the dc field distribution near the surface in such a way as to cause the hysteresis seen in Fig. 3a, assuming that the very small ac field probes predominantly the surface of the sample.[1]

Our $H_{c2}(T)$ results for $NbSe_2$ are generally in agreement with published data on larger samples of this compound.[2,4-10] However, our T_c value of 7.01 K and critical field slopes are among the lowest values reported for $NbSe_2$ (see Table I). We believe that this is due to the superior quality of our small samples, as a lower T_c implies a smaller critical field slope [see Eq. (1), below].

In Fig. 3a we show the temperature dependence of the weak coupling, clean-limit isotropic theory[27] of $H_{c2}(T)$ scaled by a constant so as to achieve an approximate best fit to the experimental data for the perpendicular orientation. Compared to the shape of $H_{c2}(T)$ predicted by the isotropic theory, both $H_{c2\perp}(T)$ and $H_{c2\parallel}(T)$ display extended linearity at low temperatures and positive, upward curvature just below T_c. The shapes of $H_{c2\perp}(T)$ and $H_{c2\parallel}(T)$ are, in fact, rather similar. The main difference is that more positive curvature near T_c is seen in $H_{c2\parallel}(T)$. Both positive curvature and/or extended linearity have previously been seen in the critical fields of anisotropic unintercalated superconductors.[4-7,28] For our samples, $H_{c2\perp}(T)$ and $H_{c2\parallel}(T)$ remain nearly linear down to the lowest temperatures measured. In addition, for some compositions, $H_{c2\parallel}(T)$ at low temperatures exceeds the simple $T = 0$ Pauli paramagnetic limiting field[29] $H_P(0) = 18.6 T_c$ kG. (This is most obvious for the composition $x = 0.05$.) The fact that $H_{c2}(T)$ exceeds $H_p(0)$ at low temperatures is not uncommon in high-field superconductors. Here it probably reflects the large amount of spin–orbit scattering expected in Nb–Ta based compounds, although it may be that a many-body-effect renormalization of the Pauli limiting field is also important.[30]

An interesting feature of the critical field data is the region of positive curvature below T_c. The inset in Fig. 3b shows $H_{c2\parallel}(T)$ near T_c on an expanded scale. This is representative of $H_{c2\perp}(T)$ as well. When examined in this detail, $H_{c2}(T)$ appears to be linear in $(T_c - T)$ over a narrow temperature interval *just* below T_c. Such linearity would be in agreement with the general expectation that $H_{c2}(T)$ should be linear in $(T_c - T)$ as $T \to T_c$. The specific heat studies were not carried out with sufficient resolution to have noted the existence of positive curvature of H_{c2}, or to establish the linearity very near T_c.

The amount of positive curvature δT_{pc} can be quantified as the difference between the measured zero-field transition temperature and the extrapolated zero-field T_c, obtained by using a straight line fit to the main linear section of the $H_{c2}(T)$ curve (the solid line in Fig. 3b). Positive curvature is seen for all compositions, and for both orientations. The δT_{pc} is twice as large for $H_{c2\parallel}(T)$ as it is for $H_{c2\perp}(T)$. It decreases by a factor of approximately two between $x = 0$ and $x = 0.20$ for both field directions.

We have found that while δT_{pc} shows systematic dependences on alloy composition and orientation, the magnitude of the positive curvature does not depend on the crystal quality, where we take the zero-field transition width as a simple measure of crystal quality. The lack of a correlation between the positive curvature and crystal quality implies that the positive curvature is not caused by sample inhomogeneities,[31] but is an intrinsic effect. A recent calculation by Machida *et al.*[32] suggested that interaction between the superconducting state and the CDW could cause positive

curvature in $H_{c2}(T)$. This calculation has been criticized, however.[33] In any case, in our samples the CDW appears to be largely suppressed for Ta contents ≥ 0.03, yet positive curvature is seen for all compositions. This experimental evidence rules out the CDW as the cause of the positive curvature in the $Nb_{1-x}Ta_xSe_2$ system. We conclude that the positive curvature of $H_{c2}(T)$ below T_c is real and intrinsic, and is not due to the charge-density wave. It appears that the positive curvature is due to Fermi surface anisotropy, as discussed in Section 5.2.

4.3. $H_{c2}(T)$: Composition-Dependent Features

Data for the critical field anisotropy $H_{c2\parallel}(T)/H_{c2\perp}(T)$ as a function of temperature are shown in Fig. 4 for a typical sample. The anisotropy is approximately constant at lower temperatures, and decreases as $T \to T_c$ over a temperature interval of ~ 2 K below T_c. This decrease of the anisotropy can be seen equivalently as a larger amount of positive curvature for $H_{c2\parallel}(T)$. The low-temperature anisotropy at a reduced temperature $t = T/T_c = 0.5$ is shown by crosses in Fig. 5 for samples with different Ta alloy compositions. (See also Table II.) The low-temperature anisotropy is a minimum for $NbSe_2$, and increases with x.

We now consider how the slope dH_{c2}/dT of the critical field curves depends on composition. There are two possible ways of defining the slope.
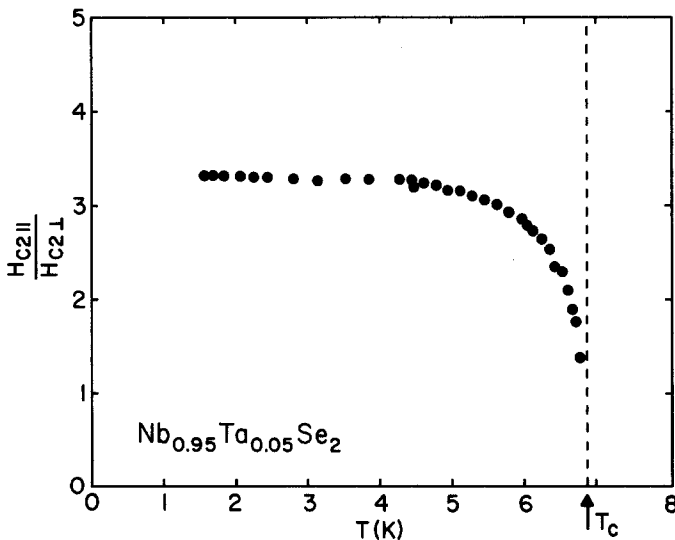

Fig. 4. The anisotropy of the critical fields as a function of temperature for a representative sample. The decrease seen as T approaches T_c is caused by the greater amount of positive curvature seen in the parallel critical field.
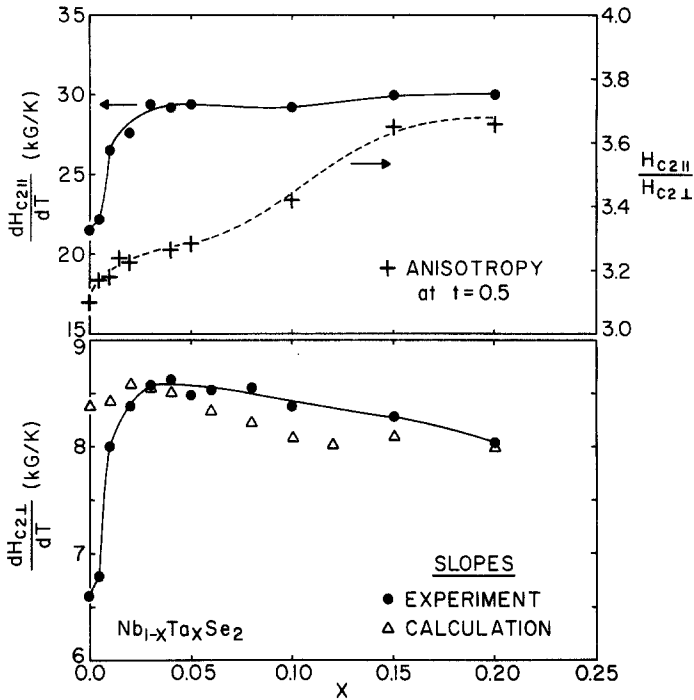
Fig. 5. The parallel and perpendicular critical field slopes dH_{c2}/dT as a function of composition. The data shown are for the slope of the main linear section of the $H_{c2}(T)$ curve. The solid lines drawn through the experimental points for the slope are intended as guides to the eye. Also shown in the upper graph, by crosses, is the anisotropy $H_{c2\parallel}/H_{c2\perp}$ as a function of composition at a reduced temperature $t = T/T_c = 0.5$. At $t = 0.5$ the anisotropy is relatively independent of temperature (see Fig. 4). Also shown in the lower figure is the perpendicular slope calculated as described in the text.

The $H_{c2}(T)$ curves clearly have a large linear region at intermediate temperatures, typically over a reduced temperature range of $t = 0.5$ to $t = 0.8$. This linear region provides the first definition of the slope. It also appears that $H_{c2}(T)$ is linear, over a much smaller temperature interval, just below T_c. This provides a second, alternative choice for the slope. For a given field direction, both of these slopes behave in a similar manner as a function of composition, differing only by a scale factor which is itself not a function of x. For $H_{c2\parallel}(T)$ the slope of the main linear section is about twice the slope just below T_c. For $H_{c2\perp}(T)$, the slope of the main linear section is approximately 4/3 the slope just below T_c. Values for both slopes are listed in Table III. There is more extensive and more accurate data for the slope of the main linear section.

TABLE III

Critical Field Slopes

Composition, at% Ta	$dH_{c2\perp}/dT$ main linear section, kG/K	$dH_{c2\perp}/dT$ just below T_c, kG/K	$dH_{c2\parallel}/dT$ main linear section, kG/K	$dH_{c2\parallel}/dT$ just below T_c, kG/K
0.0	6.60	5.00	21.5	9.2
0.5	6.79	—	22.2	9.7
1.0	8.00	5.68	26.5	11.8
2.0	8.39	7.11	27.6	13.0
3.0	8.58	7.42	29.4	12.7
4.0	8.64	7.38	29.2	14.1
5.0	8.49	7.17	29.4	15.7
6.0	8.54	6.68	—	—
8.0	8.56	7.25	—	—
10.0	8.38	5.96	29.2	16.7
15.0	8.28	6.43	30.0	14.9
20.0	8.03	6.54	30.0	—

Figure 5 shows the slope of the main linear section of H_{c2} for both field orientations as a function of x.* For both field orientations, the slope (solid dots) initially increases relatively rapidly as the Ta concentration is increased, up to $x = 0.02$. This rise is caused by changes accompanying the suppression of the CDW. For Ta concentrations large enough that the CDW is suppressed ($x \gtrsim 0.03$), the perpendicular slope decreases slightly as the Ta content is further increased, while the parallel slope increases only very slightly.

5. DATA ANALYSIS

In this section two features of the critical field data will be considered. First, we will discuss the composition dependence of the critical field slopes and the anisotropy. It is possible to qualitatively understand the dependence of these quantities on composition as being due to anisotropy effects. Second, the shape and magnitude of the experimental $H_{c2}(T)$ curves (primarily for $NbSe_2$) will be compared with calculations of $H_{c2}(T)$ using two models for the Fermi surface of $NbSe_2$. Because available theories do not treat all possible cases for anisotropic superconductors, results and concepts from the isotropic theory will be used, with suitable generalization, in the following analysis.

*The data for the slope of the main linear section will be emphasized, primarily because more data are available for this quantity, and less scatter is seen because this slope is more easily extracted from experimental data. This choice is acceptable for the semiquantitative analysis carried out in this paper.

5.1. Dependence of the Critical Field Slopes on Composition

Figure 5 shows that, as a function of composition, the critical field slopes dH_{c2}/dT display somewhat different behavior in the region $x \geq 0.03$ for the two field orientations. The perpendicular slope decreases somewhat, while the parallel slope is almost constant. To analyze the behavior for either orientation it is useful to have an explicit formula relating the slopes to the relevant material properties. An approximate relation can be obtained,[1,34]

$$\left.\frac{dH_{c2}}{dT}\right|_{T_c} = -\frac{16\pi^2}{7\zeta(3)}\frac{ck_B}{e\hbar}\frac{T_c}{\langle v_\perp^2 \rangle}\eta_{H_{c2}}(T_c)\chi^{-1}(\lambda_{tr}) \tag{1}$$

This equation is discussed in Appendix A. Band structure effects are included in the factor $\langle v_\perp^2 \rangle$, which is the Fermi surface average of the square of the component of the electron velocity in a plane perpendicular to the direction of the applied magnetic field. This dependence on the band structure is exact[34] for the weak coupling, clean ($l \to \infty$) limit (l is the electron mean free path). Here $\eta_{H_{c2}}(T_c)$ is a strong coupling correction factor, which typically varies from 1.0 to 1.2 in isotropic superconductors.[35] We assume that electron lifetime effects can be accounted for semiquantitatively by the Gor'kov function, as is exactly correct in the weak coupling isotropic limit.[29] Here

$$\lambda_{tr} = \hbar/(2\pi k_B T_c \tau) = 0.882\xi_0/l \tag{2}$$

is the normalized electron scattering rate, where τ is the electron lifetime and ξ_0 is the BCS coherence length. For $H_{c2\perp}(T)$, it is reasonable to take τ as the scattering time for transport within the layer. This assumption is made following the form of the band structure term in Eq. (1). For $H_{c2\parallel}(T)$, the choice of scattering time is less obvious.

For the perpendicular critical field slopes, it is possible to compare the experimental data with theory in a reasonably quantitative manner. If we assume that the band structure and strong coupling factors do not change significantly as the composition is varied, the slope can be written for the perpendicular field direction as

$$dH_{c2}/dT = -\alpha T_c \chi^{-1} = -\alpha T_c(1.0 + 0.895\lambda_{tr}) \tag{3}$$

Here we treat α as an adjustable constant; in Section 5.2 we consider the magnitude of $H_{c2}(T)$. The approximate form of the Gor'kov function is

$$\chi^{-1}(\lambda_{tr}) = 1.0 + 0.895\lambda_{tr} \tag{4}$$

This form is used in Eq. (3); it was obtained by a least squares fit to the exact result. χ^{-1} is exactly equal to one for $\lambda_{tr} = 0$. The constant α may be

determined from the critical field data for two compositions by using the ratio of the λ_{tr}'s given by

$$(\lambda_{tr})_1/(\lambda_{tr})_2 = (T_c\tau)_2/(T_c\tau)_1$$

For the perpendicular critical fields, the ratio of the electron lifetimes can be estimated from the basal-plane resistivities using $\rho = m/ne^2\tau$. It is convenient to use the two end compositions, NbSe$_2$ and Nb$_{0.80}$Ta$_{0.20}$Se$_2$, for this calculation. The room-temperature basal-plane resistivity of NbSe$_2$ is approximately 150 $\mu\Omega$-cm.[23,24,36,37] Assuming that it has the same electron–phonon component of the resistivity, we can estimate the room-temperature resistivity of Nb$_{0.80}$Ta$_{0.20}$Se$_2$ to be 188 $\mu\Omega$-cm. The low-temperature resistivity is obtained by dividing the room-temperature resistivity by the RRR. (We did not measure absolute resistivities, due to the very small sample size.)

For comparison with the theoretical prediction [Eq. (3)], we have chosen the slope of the main linear section of the $H_{c2}(T)$ curve, as more extensive and accurate data are available for this slope. The results are essentially independent of whether the main linear slope or the slope just below T_c is used. To make a more meaningful comparison between the behavior of NbSe$_2$ and that of the alloys, it is also useful to define a hypothetical "CDW-free" NbSe$_2$. We therefore use the perpendicular slope and T_c data of Nb$_{0.98}$Ta$_{0.02}$Se$_2$ in this comparison to define NbSe$_2$, instead of the actual NbSe$_2$ data.

With the choice of parameters discussed above we obtain $\lambda_{tr} = 0.023$ for (CDW-free) NbSe$_2$, and $\lambda_{tr} = 0.31$ for Nb$_{0.80}$Ta$_{0.20}$Se$_2$; $\alpha = 1.106$ kG/K^2. These values of λ_{tr} are listed in Table IV. Such small values for λ_{tr} are indicative of very long electron lifetimes.

The perpendicular critical field slope for intermediate compositions may be calculated from Eq. (3) by linearly interpolating between the values of λ_{tr} calculated for (CDW-free) NbSe$_2$ and Nb$_{0.80}$Ta$_{0.20}$Se$_2$. This is equivalent to assuming that the electron scattering rate τ^{-1} increases linearly with x, which is consistent with the measured dependence of the RRR on x. Figure 5 shows the perpendicular slope calculated with this assumption, along with the experimental data. The overall agreement is reasonably good

TABLE IV

Normalized Basal-Plane Transport Scattering Rates

Material	λ_{tr}	Source
NbSe$_2$	0.023 ⎫	Composition dependence of $dH_{c2\perp}/dT$
Nb$_{0.80}$Ta$_{0.20}$Se$_2$	0.31 ⎬	
NbSe$_2$	0.67	Eq. (2), τ from normal-state properties

for $x \geq 0.03$. Note that T_c decreases more significantly than the slope in this composition range, from 7.2 to 5.6 K. The dH_{c2}/dT would be expected to scale with T_c if λ_{tr} did not change [Eq. (3)]. The reasonably good agreement for $x \geq 0.03$ indicates that the dependence of the perpendicular critical fields on alloy composition is consistent with the functional dependence on T_c and the electron scattering rate predicted by Eq. (3). The agreement between theory and experiment for $dH_{c2\perp}/dT$ is poor for $x \leq 0.02$. We believe that the initial increase in the experimental slope with x is caused by band structure changes accompanying suppression of the CDW, beyond their effect on T_c. These band structure effects are not included in our model calculations, which treats only the effects of T_c and the changed electron lifetime τ.

In conclusion, our analysis of the perpendicular critical field slopes indicates that NbSe$_2$ is a very clean material for electron motion in the basal plane; alloying does not reduce the electron lifetime significantly enough to have a dramatic effect on $H_{c2\perp}(T)$. A similar analysis would be desirable for $H_{c2\parallel}(T)$. However, an analogous calculation for $H_{c2\parallel}(T)$ would require RRR data for current flow perpendicular to the layer plane and a reliable means of estimating χ^{-1} for this field orientation. This information is not currently available.

In addition to extracting λ_{tr} from the $H_{c2}(T)$ data as is done above, λ_{tr} can be calculated directly using Eq. (2), if τ can be determined from normal-state properties. Estimates of τ are possible for NbSe$_2$ using published resistivity and optical reflectivity data, as described in Appendix B. A value $\lambda_{tr} = 0.67$ is thereby obtained for basal-plane electron motion. While this still implies that NbSe$_2$ is a fairly clean superconductor, this estimate is not in good quantitative agreement with the value of λ_{tr} determined from the composition dependence of the critical field slope. This disagreement is perhaps not too worrisome, as both numerical estimates of λ_{tr} must be treated with some caution. The estimates based on the composition dependence of the slopes were obtained using the Gor'kov function, which has been derived, and is thus strictly valid, only in the isotropic limit. Also, in our calculation, band structure changes and anisotropic electron lifetime effects were ignored. On the other hand, the estimate of τ obtained in Appendix B utilizes a free-electron-type analysis, and may therefore be only qualitatively valid. Nonetheless, both estimates of λ_{tr} support the conclusion that NbSe$_2$ is a clean superconductor (i.e., the electron mean free path l is greater than the BCS coherence length ξ_0), for conduction in the layer plane. The estimates for λ_{tr} are collected in Table IV.

In addition to the effects of λ_{tr} on the composition dependence of the slopes discussed above, two additional mechanisms can affect the composition dependence of H_{c2} and the anisotropy. First, H_{c2} will be affected by

band structure changes. Second, the electron lifetime is likely anisotropic, and this anisotropy may change with x, further adding to the composition dependence of the critical field anisotropy. We will discuss band structure changes first.

NbSe$_2$ and TaSe$_2$ have the same crystal structure. TaSe$_2$ has a slightly larger c-axis lattice constant, 12.71 Å versus 12.54 Å for NbSe$_2$.[38] Thus, in TaSe$_2$ the planes of metal atoms are further apart. This may lead to more anisotropic physical properties. Indeed, the CDW onset temperature is much higher for TaSe$_2$ ($T_0 = 122$ K) than for NbSe$_2$ ($T_0 = 33.5$ K),[20] implying that TaSe$_2$ has a more two-dimensional band structure[15] than NbSe$_2$. The major changes in H_{c2} due to band structure changes appear to be in the region where the CDW is being suppressed, $x \leq 0.02$. Even for the region $x \geq 0.03$, an increase in anisotropy would be expected as the Ta concentration increases. This is what is seen in Fig. 5. An increase in anisotropy could imply a decrease in $H_{c2\perp}$ and of the slope $dH_{c2\perp}/dT$. Such a change in the perpendicular slope is in a direction opposite to the change produced by the electron lifetime effect discussed previously. If such a band structure effect were present, our previous computation of λ_{tr}, which considered only lifetime effects, would have underestimated λ_{tr}.

The composition dependence of the critical field anisotropy may also be determined, in part, by effects of the *anisotropy* of the electron lifetime. It appears that for NbSe$_2$, $H_{c2\parallel}$ is closer to the dirty limit (the effective λ_{tr} is larger) than is $H_{c2\perp}$. This view is argued by Ikebe *et al.*[10] (The appropriate definition of λ_{tr} appears to involve an average of τ^{-1} in the plane perpendicular to the field direction.) Thus, while alloying increases τ^{-1} and H_{c2}, the fractional increase of $H_{c2\perp}$ would be smaller than that of $H_{c2\parallel}$, since χ^{-1} is relatively insensitive to increases of λ_{tr} for small values of λ_{tr}, as is the case for $H_{c2\perp}$. The moderate increase in anisotropy with x, seen in the upper graph of Fig. 5, may thus be due to this anisotropic electron lifetime effect. With the present knowledge of the normal state properties of the alloys, it is not possible to distinguish which of these mechanisms is in fact dominant.

5.2. $H_{c2}(T)$ Calculations for NbSe$_2$: Magnitude and Shape

This section describes the calculation of the magnitude and temperature dependence of $H_{c2\perp}(T)$ and $H_{c2\parallel}(T)$ for NbSe$_2$ for several model Fermi surfaces. Nearly all previous comparisons of experimental $H_{c2}(T)$ data with theory for the unintercalated layered compounds have used the anisotropic Ginzburg–Landau (GL) theory. The GL theory is valid only near T_c, where it predicts that $H_{c2}(T)$ is linear in $(T_c - T)$. Thus, the anisotropic Ginzburg–Landau theory is incapable of explaining the shape of the observed $H_{c2}(T)$

curves over the full temperature range below T_c. We have therefore performed calculations of $H_{c2}(T)$ using a microscopic theory valid for all temperatures. In addition, we have used realistic Fermi surface models in these microscopic theory calculations. We have previously found that simpler model Fermi surfaces, such as a single ellipsoid, do not lead to H_{c2} predictions that exhibit all the features of the experimental data.[1]

The calculations we have carried out use a clean-limit, weak coupling formalism developed by Butler.[34] This formalism is valid for all $T \le T_c$. Anisotropy is included in that the shape of the Fermi surface and the electron velocity on the Fermi surface can be specified arbitrarily. We refer to these factors together as Fermi surface anisotropy. Gap anisotropy has not been included in the calculations. A theory of $H_{c2}(T)$ incorporating both Fermi surface and gap anisotropy was derived by Youngner and Klemm.[39] Their results show that gap anisotropy can produce effects that are qualitatively like those produced by Fermi surface anisotropy. Thus, it is difficult to estimate quantitatively the effect of omitting gap anisotropy from the calculations. Butler calculated H_{c2} for Nb and found that gap anisotropy was not needed to explain $H_{c2}(T)$ for that system. Butler found that the orientation and temperature dependence of $H_{c2}(T)$ was correctly predicted using the known band structure of Nb. Niobium is a cubic material and is, of course, much less anisotropic than $Nb_{1-x}Ta_xSe_2$. It appears that the omission of gap anisotropy effects in our analysis may be acceptable.

Spin effects are also not included in our analysis. Spin effects appear to be unimportant for the perpendicular orientation, and likely are also unimportant for the parallel orientation. (No currently available theory includes both spin and anisotropy effects, in any event.) There is no evidence of Pauli paramagnetic limiting in the $H_{c2\parallel}(T)$ data, where $H_{c2\parallel}(0) \simeq H_P(0)$. This implies that spin effects are unimportant for $H_{c2\parallel}(T)$. In the perpendicular field direction, the experimental low-temperature value of $H_{c2\perp}(0)$ is only one-third of $H_P(0)$, so that spin effects are clearly unimportant for this field orientation.

In addition to the effects considered so far in this section, the effects on $H_{c2}(T)$ of finite electron lifetime and of strong electron–phonon coupling should be included. To do this, we use the multiplicative correction factors from the isotropic theory, given in Eq. (1) for the slope.* The estimate obtained in Appendix B for the normalized electron scattering rate $\lambda_{tr} = 0.67$ will be used for calculating χ^{-1}. $\chi^{-1}(0.67) = 1.58$. This value of λ_{tr} is an upper limit, so that $\chi^{-1}(0.67) = 1.58$ is also an upper limit.

---

*In the isotropic theory, the Gor'kov function determines the electron lifetime dependence of only the critical field slopes. However, the shape of the critical fields [i.e., $h_{c2}(T)$] varies only slightly from the clean limit to the dirty limit, so to lowest order, the Gor'kov function can also be taken to describe the electron lifetime dependence of $H_{c2}(T)$.

Strong electron–phonon coupling effects are important primarily because the Fermi velocity from the band structure calculation must be renormalized by a factor of $(1 + \lambda_{ep})^{-1}$ before it can be used in the critical field calculations.[34] (The reason for this is discussed in Appendix B.) It is acceptable to perform the calculations using band-structure electron velocities, if one then multiplies the resulting (clean-limit) $H_{c2}(T)$ by $(1 + \lambda_{ep})^2$. (This is because $H_{c2} \propto v_F^{-2}$ in the clean limit.) A multiplicative strong coupling correction factor $\eta_{H_{c2}}(T)$ should also be included* as in Eq. (1). The total correction factor multiplying the results of the clean-limit, weak coupling (CLWC) calculation of $H_{c2}(T)$ is thus given by

$$H_{c2}(T) = (1 + \lambda_{ep})^2 \chi^{-1}(\lambda_{tr}) \eta_{H_{c2}}[H_{c2}(T)]^{CLWC} \tag{5}$$

where $[H_{c2}(T)]^{CLWC}$ is given by the Butler calculation using band-structure Fermi velocities. We estimate $\lambda_{ep} = 1.5$ (Appendix B), and take $\eta_{H_{c2}}(T_c)$ to be 1.14, using the results of a model calculation by Masharov.[40] Because of the directional nature of some of the normal-state properties used to obtain these correction factors, they are only valid for $H_{c2\perp}(T)$.

The simplest model of an anisotropic Fermi surface is an ellipsoid of rotation. $H_{c2}(T)$ can be calculated for such a Fermi surface model using the effective mass approximation, given in Eq. (6), below. Parameters of the ellipsoid, m and γ, can be chosen so that for any one field orientation the calculated $H_{c2}(T)$ has the correct magnitude and displays the features of positive curvature and extended linearity. The Fermi surface must be compressed along the field axis for $H_{c2}(T)$ to display these features. However, we have found that it is not possible to obtain for *both* field orientations agreement with experiment for the magnitudes and for the existence of extended linearity and positive curvature, if one uses only a *single* ellipsoidal Fermi surface. Because of this limitation, it is necessary to consider more complicated Fermi surface models, as discussed below. We note that the single-ellipsoid Fermi surface model is closely related to the Fermi surface model used by Youngner and Klemm,[39] who were able to fit perpendicular field data for NbSe$_2$ using a Fermi surface model consisting of a distorted sphere. It is unlikely that the parallel field data could also be fit using a model with that same distorted sphere.

We next consider the real, calculated Fermi surfaces of NbSe$_2$ for calculation of $H_{c2\perp}$. The band structure of NbSe$_2$ has been calculated by Mattheiss[41] using the augmented-plane-wave method. The band structures of both NbSe$_2$ and TaSe$_2$ have been calculated by Wexler and Woolley[42] using a layer technique. The Wexler and Woolley results for NbSe$_2$ and

---

*We assume that $\eta_{H_{c2}}(T) = \eta_{H_{c2}}(T_c)$.

TaSe$_2$ are very similar (for a detailed comparison, see Ref. 42). The calculations by Wexler and Woolley (and also by Mattheiss) are nonrelativistic, so that they may underestimate the difference between Nb-based and Ta-based compounds.

The band structure calculations show that the energy bands at the Fermi level are primarily derived from transition-metal d orbitals. The layer technique used by Wexler and Woolley is particularly well suited to determining the Fermi surface since it can produce constant-energy surfaces in k-space. In contrast, the calculation by Mattheiss only yields the energy eigenvalues at eight high-symmetry points in the Brillouin zone, so that the Fermi surface must be determined by a less accurate interpolation technique. For NbSe$_2$ and TaSe$_2$ Wexler and Woolley find that the Fermi surface consists of open, undulating cylinders parallel to the k_z axis (perpendicular to the basal plane). In the hexagonal Brillouin zone there is one cylinder passing through the center of the zone, and six symmetry-related cylinders at the zone corners. This Fermi surface is shown schematically in Fig. 6.

The Wexler and Woolley band structure calculation is for room-temperature NbSe$_2$ and thus does not include the effects of the CDW on the band structure. The CDW appears to impose a rather weak perturbation on the band structure of NbSe$_2$, in that the changes seen in most normal-state properties at the CDW transition are rather small.* The CDW does affect T_c and the critical field slopes, but not dramatically. From the observed suppression of T_c it can be estimated (using the BCS equation for the transition temperature) that the CDW causes a 2% reduction in the density of states at the Fermi energy. It thus appears useful, as a first approximation, to ignore the CDW and calculate $H_{c2}(T)$ using the available Wexler and Woolley Fermi surface model.†

Our calculation of H_{c2} using the Wexler and Woolley Fermi surface is not intended primarily as a quantitative test of the Wexler and Woolley results. Rather, we use their results for the quasicylindrical Fermi surface as a model Fermi surface, and ask whether those qualitative Fermi surface features can lead to the features seen in the experimental $H_{c2\perp}$ results.

Figure 6 shows $H_{c2\perp}(T)$ calculated from the Wexler and Woolley Fermi surface as solid dots. The multiplicative correction factors of Eq. (5) have been incorporated. Experimental data for $H_{c2\perp}(T)$ are also shown, as a solid line. The calculated magnitude is clearly too small. Though difficult

---

*At the CDW onset in NbSe$_2$, effects on the order of 5% are seen in the resistivity,[43] the heat capacity,[43] and the electron distribution as determined from NMR data.[44] However, the sign of the Hall coefficient is observed to change, indicating that the Fermi surface connectivity is altered.[22,37]

†To calculate $H_{c2}(T)$ requires values for the electron velocity at all points on the Fermi surface. Professor A. M. Woolley kindly provided us with unpublished data concerning the energy dependence of the constant-energy surfaces near E_F, from which the velocity was calculated.
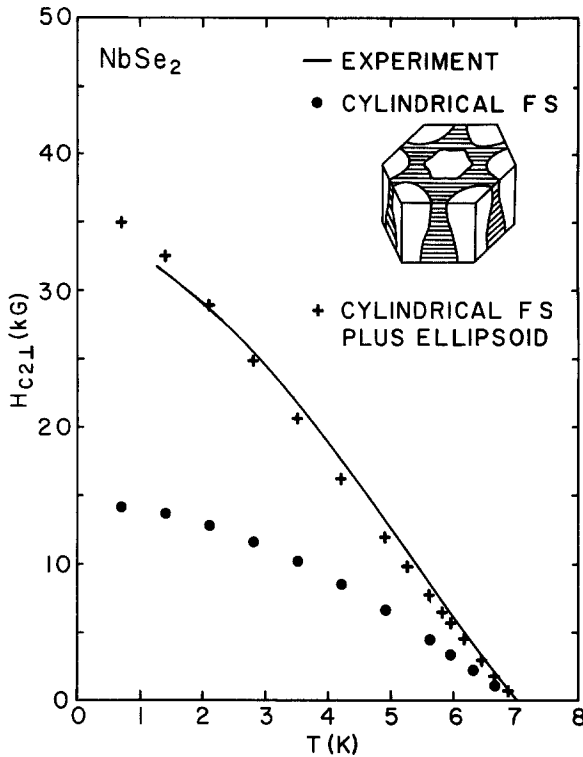
Fig. 6. Experimental $H_{c2\perp}(T)$ curve of $NbSe_2$, along with $H_{c2\perp}(T)$ calculated using two Fermi surface models: the cylindrical Wexler and Woolley Fermi surface, and a model incorporating the Wexler and Woolley cylinders plus a closed ellipsoidal piece. A sketch of the hexagonal Brillouin zone is included, showing the several open cylindrical Fermi surface pieces calculated by Wexler and Woolley.[42] (The additional ellipsoidal Fermi surface piece is not shown.)

to see on this plot, the experimental data display both positive curvature and extended linearity, while the calculated $H_{c2\perp}(T)$ curve displays neither. Thus, neither the magnitude nor the shape of the calculated $H_{c2\perp}(T)$ agrees well with the experimental data.

The agreement between theory and experiment can be significantly improved by postulating the existence of an additional Fermi surface piece. Graebner and Robbins[45] noted that their de Haas–van Alphen results for $NbSe_2$ were consistent with the existance of a small, flat Fermi surface piece lying in the basal plane. It has been suggested[46] that such a piece could result from an improved band structure calculation that took account of

charge transfer from the Nb atoms to the more electronegative Se atoms, i.e., making the calculation more self-consistent.

The $H_{c2}(T)$ calculations have been repeated using a Fermi surface model consisting of the Wexler and Woolley cylinders plus a small ellipsoid. The result is also shown in Fig. 6, with crosses. The ellipsoid used here is treated in the effective mass model, for which

$$E = \frac{\hbar^2}{2m} \left[k_x^2 + k_y^2 + \left(\frac{k_z}{\gamma} \right)^2 \right] \tag{6}$$

The effective mass m is taken to be six times the free-electron mass; $\gamma = 0.6$. These parameters were chosen to provide a good fit to the experimental H_{c2} data. The major axes of the ellipsoid lie in the k_x–k_y (layer) plane and are equal to $0.754 \, Å^{-1} = 2.6 a_0^{-1}$ ($a_0 = 3.45 \, Å$ is the lattice constant). The minor axis is along the k_z axis and is 0.6 times the major axis, $0.452 \, Å^{-1}$. The diameter of the inner cylinder in the Wexler and Woolley Fermi surface is approximately $0.90 \, Å^{-1} = 3.1 a_0^{-1}$, so that the added ellipsoid does not intersect the cylinders.

The $H_{c2\perp}(T)$ calculated using this model of the Fermi surface is approximately of the experimental magnitude and also displays both the positive curvature and extended linearity seen in the experimental data. The positive curvature and extended linearity for this field orientation are due to the ellipsoidal piece of the Fermi surface.

The parameters of the additional ellipsoid may be physically reasonable, although its size is considerably larger than that proposed by Graebner and Robbins.[45,*] They found a diameter equal to $0.344 \, Å^{-1}$ and a thickness of $0.054 \, Å^{-1}$. The ellipsoid used here has a diameter of $0.754 \, Å^{-1}$ and a thickness of $0.452 \, Å^{-1}$. Since $H_{c2}(T)$ is calculated using a Fermi surface average [as in Eq. (1)], adding a small ellipsoid of the size proposed by Graebner and Robbins would not have had much effect on the critical fields, because the surface area of the cylinders is much larger. The need to use such a large ellipsoid to obtain agreement of theory with experiment may well indicate that the cylindrical parts of the Fermi surface model require modification. If this is the case, the required ellipsoidal Fermi surface piece could well be smaller. Effects of gap anisotropy may also be important. Still, we can tentatively conclude that the experimental perpendicular critical

---

*The CDW in NbSe$_2$ is almost commensurate.[10] If it was exactly commensurate, the high-temperature band structure (no CDW) could be folded into the smaller low-temperature Brillouin zone to approximate the band structure in the CDW state. According to Graebner and Robbins,[45] such a procedure will not produce an ellipsoidal Fermi surface piece as suggested by the de Haas–van Alphen results. Graebner and Robbins used the band structure calculated by Mattheiss.[41]

fields are more consistent with a Fermi surface that includes a flattened, closed piece than with a Fermi surface that consists entirely of open, undulating cylinders.

We have also calculated $H_{c2\parallel}(T)$ using the two Fermi surface models—cylinders, and cylinders plus ellipsoid. It is not easy to compare the magnitude of these results to experimental data, since for the parallel field orientation it is not possible to estimate the correction factors to account for the electron lifetime and strong coupling effects. For both Fermi surface models, the calculated $H_{c2\parallel}(T)$ curves display positive curvature and extended linearity. Both results can be approximately fit to the experimental data using reasonable correction factors. For the parallel field orientation, the added ellipsoid has a less dramatic effect on the calculated critical fields. The level of agreement between the experimental shapes of $H_{c2\parallel}(T)$ and those predicted by theory is like that seen in Fig. 6 for the perpendicular orientation with the Fermi surface model that includes the ellipsoid. The scale factors required for the parallel field case are larger than the correction factor estimated for the $H_{c2\perp}(T)$ calculation. for the Fermi surface model that includes the ellipsoid, the parallel field scale factor is 2.5; for the Wexler and Woolley Fermi surface model alone, the scale factor is 3.6. these multiplicative factors would be consistent with an anisotropic electron lifetime effect, since a smaller interlayer electron lifetime would produce a larger correction factor, through $\chi^{-1}(\lambda_{tr})$, for $H_{c2\parallel}(T)$.

6. SUMMARY AND CONCLUSIONS

In this paper we have presented measurements of $H_{c2\perp}(T)$ and $H_{c2\parallel}(T)$ for high-quality, single-crystal samples of the compounds Nb$_{1-x}$Ta$_x$Se$_2$ $(0 \leq x \leq 0.20)$. A large number of different compositions have been studied, allowing a thorough characterization of how the critical fields vary with composition. Starting from pure NbSe$_2$, T_c initially increases when a small fraction of the Nb atoms are replaced by Ta atoms. This is due to the suppression of the charge-density wave by lattice disorder.

Both $H_{c2\perp}(T)$ and $H_{c2\parallel}(T)$ display positive curvature below T_c and extended linearity at low temperature. The positive curvature below T_c is definitely an intrinsic phenomenon and is not due to the charge-density wave. The amount of positive curvature observed is a weak function of sample composition, but not of crystal quality. These conclusions do not depend on how $T_{c2}(H)$ is defined. There are, in general, several mechanisms that can cause positive curvature and extended linearity. In the layered compounds studied, positive curvature and extended linearity appear to both be caused by Fermi surface anisotropy. Evidence in support of this conclusion comes from our critical field calculations, which show that a

plausible Fermi surface is capable of producing both positive curvature and extended linearity for both field orientations.

The critical fields of the alloy series do not change greatly as a function of composition. The changes that are seen can be explained quantitatively as resulting from changes in T_c and changes in the electron lifetime with alloying, perhaps augmented by small band structure changes. For x in the range $0 < x \lesssim 0.02$ there is the additional factor that the CDW is being suppressed with substitution of Ta for Nb. For $x > 0.02$, $H_{c2\perp}(T)$ does not depend strongly on x. The apparently small effect on H_{c2} of changes in the electron lifetime as x goes from 0.02 to 0.2 may be surprising, given the relatively large resistivity of $NbSe_2$ and the rapid drop in the RRR that occurs as the Ta content is increased. However, our quantitative analysis of the composition dependence of the perpendicular slope shows that the small observed effect of Ta alloying can be fairly well understood as being due to $NbSe_2$ being a very clean material, with $\lambda_{tr} \ll 1$. The situation is not completely and quantitatively resolved, however, as the two different values of λ_{tr} in Table IV indicate. For the future, it would be most useful to have accurate measurements of various normal-state properties of the alloy compounds to provide more accurate estimates of the electron lifetimes. Of greatest importance would be measurements of the resistivity for current flow both perpendicular and parallel to the layer plane.

We have presented evidence that $NbSe_2$ is a clean superconductor, at least as regards electron motion in the layer plane. This conclusion is based on the variation of $H_{c2\perp}(T)$ with composition and upon the basal-plane electron lifetime obtained from normal-state properties. The reasoning we have used to reach this conclusion is based on concepts from the isotropic theory of $H_{c2}(T)$. It would, of course, be extremely useful to also have available a microscopic theory of $H_{c2}(T)$ for anisotropic systems that incorporates electron lifetime effects. Such a theory would allow us to make a much more rigorous analysis of critical field data of $Nb_{1-x}Ta_xSe_2$ than is possible at present.

Our calculations of $H_{c2\perp}(T)$ and $H_{c2\parallel}(T)$ for $NbSe_2$ used two models of the Fermi surface: that calculated by Wexler and Woolley, a cylindrical Fermi surface, and a model with the Wexler and Woolley cylinders and an additional closed, ellipsoidal piece. The weak coupling, clean-limit theory of Butler has been used to calculate $H_{c2}(T)$, with strong coupling and electron lifetime effects included via multiplicative correction factors taken over from the isotropic theory. These correction factors can only be evaluated with certainty for the perpendicular critical field. The results of the $H_{c2}(T)$ calculations indicate that a Fermi surface model that includes a closed ellipsoidal piece in addition to the open cylinders of the Wexler and Woolley model is in better agreement with experiment than is a Fermi surface model

that consists only of the open cylinders. The conclusion that a closed Fermi surface piece is required is in qualitative agreement with de Haas–van Alphen results[45] and theoretical speculation.[46] For the future, it would be interesting to compare the results of a relativistic, self-consistent band structure calculation with this modified Fermi surface model. Ideally, such a calculation would include the effect of the CDW. It is certain for the future that further analysis of the experimental results presented here will be possible as theoretical advances are made for treating the properties of anisotropic superconductors.

APPENDIX A

This appendix discusses an approximate formula for the slope dH_{c2}/dT below T_c for anisotropic superconductors. In the weak coupling, clean limit it can be shown that the slope is given by[1,34]

$$\frac{dH_{c2}}{dT}\bigg|_{T_c} = -\frac{16\pi^2}{7\zeta(3)}\frac{ck_B}{e\hbar}\frac{T_c}{\langle v_\perp^2 \rangle} \tag{A1}$$

$v_\perp^2$ is the square of the component of the electron velocity in a plane perpendicular to the direction of the magnetic field. The angular brackets indicate a Fermi surface average (see, e.g., Ref. 47). This differs from the corresponding isotropic formula[29] in that v_F^2 in that formula is replaced by $(3/2)\langle v_\perp^2 \rangle$. For a spherical Fermi surface $\langle v_\perp^2 \rangle = (2/3)v_F^2$, so the isotropic result is recovered. Finite electron lifetime effects can be approximately included by multiplying Eq. (A1) by the inverse Gor'kov function $\chi^{-1}(\lambda_{tr})$. This approach is exact in the weak coupling isotropic theory. Here it is only an approximation since, e.g., electron scattering will influence the Fermi surface average. However, for reasonably clean materials (as are considered in this paper) this approximation should be valid.

APPENDIX B

To calculate the quantity $\lambda_{tr} = \hbar/(2\pi k_B T_c \tau)$ directly for NbSe$_2$ requires an estimate for the electron lifetime τ. An estimate for basal-plane electron motion can be obtained as follows. The room-temperature electron lifetime has been determined to be $\tau = 2.5 \times 10^{-15}$ sec in optical reflectivity studies.[48] The same value can be obtained from the resistivity using the formula $\rho = m/n e^2 \tau$. We use a resistivity[23,24,36,37] of 150 $\mu\Omega$-cm, an electron density[48] $n = 1.55 \times 10^{28}$ m^{-3}, and a mass of 1.6 times the free-electron value, as determined from the optical reflectivity measurements. To calculate λ_{tr}, the low-temperature lifetime is required. The low-temperature lifetime is larger

than the room-temperature value by a factor[49] of RRR($1 + \lambda_{ep}$), where λ_{ep} is the electron–phonon coupling constant and RRR is the residual resistance ratio, equal to 41 for our $NbSe_2$ crystals. This result follows directly from the formula $\rho = m/n e^2 \tau$, where for $T < \theta_D$ (the Debye temperature), m, τ, and v_F are renormalized from their (room-temperature) band structure values by the electron–phonon interaction,[49] as given by[49]

$$m = (1 + \lambda_{ep}) m_{bs} \qquad\qquad (B1)$$

$$\tau = (1 + \lambda_{ep}) \tau_{bs} \qquad\qquad (B2)$$

$$v_F = (1 + \lambda_{ep})^{-1} v_{F_{bs}} \qquad\qquad (B3)$$

Here bs denotes the band structure value. In effect λ_{ep} vanishes for $T > \theta_D$.[49] The Debye temperature θ_D is about 220 K for the compounds $Nb_{1-x}Ta_xSe_2$.[50]

We use a measured value RRR = 41 for $NbSe_2$. The λ_{ep} is estimated to be 1.5 from resistivity, optical reflectivity, and heat capacity data.[1] (This is a fairly large value for λ_{ep}, but it is not unreasonable given the strong electron–phonon interaction implied by a room-temperature resistivity of 150 $\mu\Omega$-cm with a RRR = 41.) With $T_c = 7.01$ K, we finally obtain $\lambda_{tr} = 0.67$.

We note that a previous computation of λ_{tr} in Ref. 2 yielded a value of $\lambda_{tr} = 0.13$ for $NbSe_2$. That estimate was based on a number of assumptions. While those assumptions appeared reasonable, we do not consider that result to be as reliable as the estimates in the present work. In any case, the estimates of λ_{tr} in Ref. 2 and in this paper are all in agreement with the conclusion that $NbSe_2$ is a clean superconductor.

REFERENCES

1. B. J. Dalrymple, Ph. D. Thesis, Yale University (1983); available from University Microfilms, Ann Arbor, Michigan.

2. D. E. Prober, R. E. Schwall, and M. R. Beasley, *Phys. Rev. B* **21**, 2717 (1980).
3. R. V. Coleman, G. K. Eiserman, S. J. Hillenius, A. J. Mitchell, and J. L. Vincent, *Phys. Rev. B* **27**, 125 (1983).
4. S. Foner and E. J. McNiff, Jr., *Phys. Lett.* **45A**, 429 (1973).
5. N. Toyota, H. Nakatsuji, K. Noto, A. Hoshi, N. Kobayashi, Y. Muto, and Y. Onodera, *J. Low Temp. Phys.* **25**, 485 (1976).
6. H. A. Leupold, F. Rothwarf, J. J. Winter, J. T. Breslin, R. L. Ross, and T. R. AuCoin, *J. Appl. Phys.* **45**, 5399 (1974).
7. R. E. Schwall, G. R. Stewart, and T. H. Geballe, *J. Low Temp. Phys.* **22**, 557 (1976).
8. P. Garoche, J. J. Veyssie, P. Mamuel, and P. Moline, *Solid State Commun.* **19**, 455 (1976).
9. P. deTray, S. Gygax, and J. P. Jan, *J. Low Temp. Phys.* **11**, 421 (1973).
10. M. Ikebe, K. Katagiri, K. Noto, and Y. Muto, *Physica* **99B**, 209 (1980).
11. H. Teichler, in *Anisotropy Effects in Superconductors*, H. W. Weber, ed. (Plenum Press, New York, 1977), p. 7.
12. R. C. Morris, R. V. Coleman, and R. Bhandari, *Phys. Rev. B* **5**, 895 (1972).
13. P. Entel and M. Peter, *J. Low Temp. Phys.* **22**, 613 (1976).
14. K. Takanaka, *J. Phys. Soc. Jpn.* **52**, 2173 (1983).
15. J. A. Wilson, F. J. DiSalvo, and S. Mahajan, *Adv. Phys.* **24**, 117 (1975).
16. N. E. Lewis, T. E. Leinhardt, and J. G. Dillard, *Mat. Res. Bull.* **10**, 967 (1975).
17. B. J. Dalrymple, S. Mroczkowski, and D. E. Prober, *J. Crystal Growth*, to appear.
18. J. R. Clem, in *Low Temperature Physics LT-13*, K. D. Timmerhaus, W. J. O'Sullivan, and E. F. Hammel, eds. (Plenum Press, 1974), Vol 3, p. 102; J. F. Bussiere, *Phys. Lett.* **58A**, 343 (1976).
19. B. J. Dalrymple and D. E. Prober, *Rev. Sci. Instrum.*, **55**, 598 (1984).
20. D. E. Moncton, J. D. Axe, and F. J. DiSalvo, *Phys. Rev. B* **16**, 801 (1977).
21. T. F. Smith, L. E. Delong, A. R. Moodenbaugh, T. H. Geballe, and R. E. Schwall, *J. Phys. C* **5**, L230 (1972).
22. D. J. Huntley and R. F. Frindt, *Can. J. Phys.* **52**, 861 (1974).
23. J. R. Long, S. P. Bowen, and N. E. Lewis, *Solid State Commun.* **22**, 363 (1977).
24. N. Noto, S. Morohashi, K. Arikawa, and Y. Muto, *Physica* **99B**, 204 (1980).
25. B. P. Clayman and R. F. Frindt, *Solid State Commun.* **9**, 1881 (1971).
26. E. Revolinsky, G. A. Spiering, and D. J. Beerntsen, *J. Phys. Chem. Solids* **26**, 1029 (1965).
27. E. Helfand and N. R. Werthamer, *Phys. Rev.* **147**, 288 (1966).
28. S. J. Williamson, *Phys. Rev. B* **2**, 3545 (1970); M. R. Skokan, R. C. Morris, and W. G. Moulton, *Phys. Rev. B* **13**, 1077 (1976).
29. T. P. Orlando, E. J. McNiff, Jr., S. Foner, and M. R. Beasley, *Phys. Rev. B* **19**, 4545 (1979).
30. T. P. Orlando and M. R. Beasley, *Phys. Rev. Lett.* **46**, 1598 (1981).
31. W. L. Carter, S. J. Poon, G. W. Hull, Jr., and T. H. Geballe, *Solid State Commun.* **39**, 41 (1981).
32. K. Machida, T. Koyama, and T. Matsubara, *Phys. Rev. B* **23**, 99 (1981).
33. G. S. Grest, K. Levin, and M. J. Nass, *Phys. Rev. B* **25**, 4562 (1982).
34. W. H. Butler, *Phys. Rev. Lett.* **44**, 1516 (1980).
35. D. Rainer and G. Bergmann, *J. Low Temp. Phys.* **14**, 501 (1974).
36. J. Edwards and R. F. Frindt, *J. Phys. Chem. Solids* **32**, 2217, (1971).
37. H. N. S. Lee, H. McKinzie, D. S. Tannhauser, and A. Wold, *J. Appl. Phys.* **40**, 602 (1969).
38. E. Revolinsky, B. E. Brown, D. J. Beerntsen, and C. H. Armitage, *J. Less-Common Metals* **8**, 63 (1965).
39. D. W. Youngner and R. A. Klemm, *Phys. Rev. B* **21**, 3890 (1980).
40. N. F. Masharov, *Sov. Phys. Solid State* **16**, 1524 (1975).
41. L. F. Mattheiss, *Phys. Rev. B* **8**, 3719 (1973).
42. G. Wexler and A. M. Woolley, *J. Phys. C* **9**, 1185 (1976).
43. J. M. E. Harper, T. H. Geballe, and F. J. Disalvo, *Phys. Rev. B* **15**, 2943 (1977).
44. C. Berthier, D. Jerome, and P. Molinie, *J. Phys. C.* **11**, 797 (1978).
45. J. E. Graebner and M. Robbins, *Phys. Rev. Lett.* **36**, 422 (1976).
46. N. J. Doran, *Physica* **99B**, 227 (1980).
47. K. H. Berthel and B. Pietrass, *J. Low Temp. Phys.* **33**, 127 (1978).

48. S. S. P. Parkin and A. R. Beal, *Philos. Mag. B* **42**, 627 (1980); R. Bachmann, H. C. Kirsch, and T. H. Geballe, *Solid State Commun.* **9**, 57 (1971); J. A. Benda, R. E. Howard, and W. A. Phillips, *J. Phys. Chem. Solids* **35**, 937 (1974).
49. G. Grimvall, *The Electron–Phonon Interaction in Metals* (North-Holland, 1981); *Phys. Scripta*, **14**, 63 (1976); W. H. Butler, in *Treatise on Material Science and Technology*, F. Y. Fradin, ed. (Academic Press, 1981), Vol. 21, p. 165.
50. N. Kobayashi, K. Noto, and Y. Muto, *J. Low Temp. Phys.* **27**, 217 (1977); M. H. Van Maaren and H. B. Harland, *Phys. Lett.* **29A**, 571 (1969).